31

HF Skywave Radar Performance in the Tsunami Detection and Measurement Role

Stuart Anderson
Defence Science and Technology Organisation
Australia

1. Introduction

The severity of the threat posed to coastal communities by tsunamis has come into prominence following the event of Boxing Day 2004 when some 230,000 people lost their lives. Many countries have set up tsunami warning systems, or augmented existing systems, but overwhelmingly these derive their information from seismic monitoring stations which detect and locate earthquakes, not measurements of any resulting tsunamis. As a consequence, the false alarm rate is high, which leads to a loss of credibility of issued warnings and an inclination on the part of the public to ignore them.

Given our limited inability to predict whether a given seismic event will generate a tsunami, let alone provide quantitative information concerning its amplitude, researchers have sought to develop sensors which can provide reliable and accurate answers to these questions. These sensors fall into two categories. First, there are in situ devices, such as tsunameter stations and tide gauges, which monitor the ocean surface elevation at a single location. The Indian Ocean presently has only a handful of tsunameter stations, the Pacific Ocean more than thirty, as shown in Figure 1. These instruments use bottom-mounted pressure recorders to obtain time series data which can be subjected to spectrum analysis to separate low frequency, long wavelength signals of tsunamis from the much stronger responses due to wind waves and swell. Claimed sensitivity for advanced systems approaches ± 1 cm in 6000 m water depth, however given that the amplitude of a potentially dangerous tsunami may be only a few centimetres in the deep ocean, while waves and swell often exceed several metres in height, the potential for error is high. Moreover, the cost of a single deep sea tsunameter station, together with its deployment may easily exceed $250,000. Accordingly, the overall cost of a reasonably dense network would be enormous.

The second category of sensors embraces those which employ remote sensing techniques, either from space, in the form of satellite-borne altimeters, or from land, in the form of HF radars. Each of these remote sensing technologies has demonstrated that it is capable of measuring one or more of the various signatures which characterise a tsunami, with a precision which offers meaningful quantitative estimates of the amplitude of the disturbance. For example, the JASON-1 and Topex/Poseidon satellites which passed over the Boxing Day tsunami while it was propagating across the north-east Indian Ocean were able to detect the associated change in surface elevation and, in the case of Jason-1, a correlated variation in surface roughness inferred from the microwave radar scattering coefficient (Godin et al, 2009).

Allowing that there are several types of sensor capable of detecting a tsunami and measuring some parameter indicative of its magnitude, there remains the issue of spatial and temporal sampling. Ideally real-time detection, monitoring and characterisation of tsunamis requires ocean basin scale spatial coverage at a resolution significantly finer than the spatial scale of the disturbance itself (which has a wavelength typically of the order of 100 km), together with persistent observation with a temporal sampling interval measured in minutes rather than hours. This does not mean that the instantaneous field-of-view of the sensor system need span the entire ocean basin; rather, it should have the ability to survey the entire region of interest, preferably with a 'random-access' capability so that it can respond immediately to cueing and enable it to follow the propagating disturbance. Apart from an impractically large constellation of space-borne sensors, or an even denser network of tsunameters, only HF skywave radar appears to possess the desired combination of spatial and temporal sampling (Anderson, 2008). Overlaid on Figure 1 are the nominal coverage sectors of the three major Australian HF skywave radars.

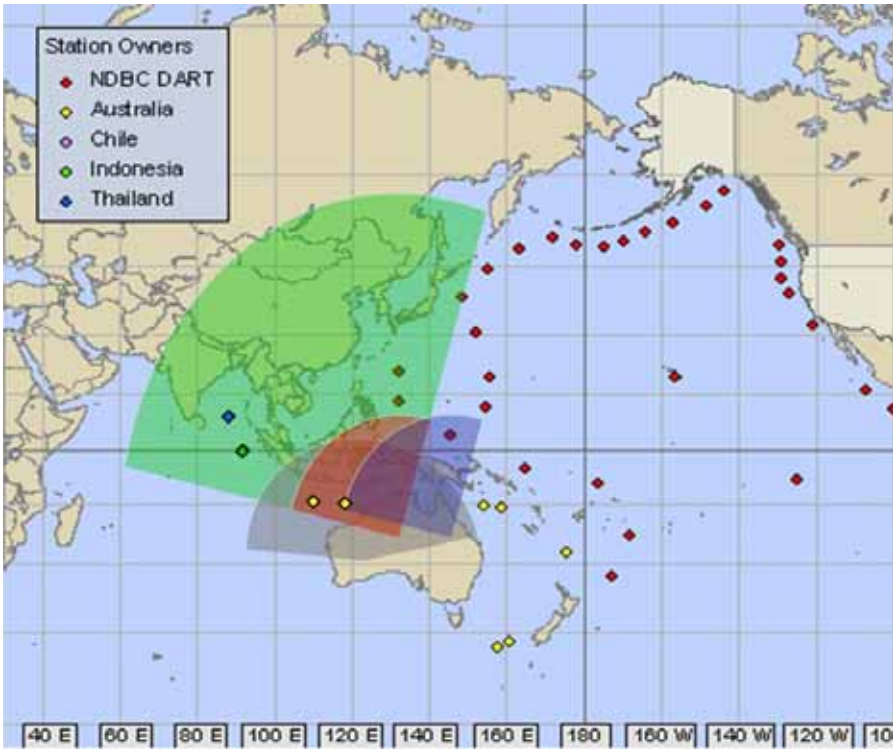

Fig. 1. The geographical distribution of deep-ocean tsunameters (NOAA, 2010) compared with the nominal coverage of the major Australian OTH radars (small sectors) and the low resolution frequency management system coverage for the central radar (large sector)

The possibility that tsunamis might be detected via quasi-vertical HF sounding of the disturbances they cause in the ionosphere was first raised in the 1970's (Hines, 1972; Najita et al, 1974), though in neither case were any of the practical difficulties of implementation

addressed. Some of these issues were subsequently examined (Peltier & Hines, 1976), again in the context of a network of vertical incidence sounders, concluding that a tsunami warning capability was feasible, subject of course to suitable geographical disposition of the sounders. The idea of employing HF skywave radar in a tsunami warning role was proposed much later (Anderson, 1994), when it was noted that the oblique propagation geometry afforded a very wide coverage from a single site, eliminating the need for a network of sounders and islands on which to situate them, and introducing the prospect of mapping the tsunami-induced ionospheric disturbances continuously in space and time.

Following the Boxing Day Sumatran tsunami of 2004, interest in developing new techniques for tsunami detection increased enormously. One line of enquiry focussed on the application of tomographic inversion of total electron content (TEC) data from dense networks of Global Positioning System (GPS) receivers to image ionospheric disturbances arising from seismic phenomena via the mechanism of upwardly-propagating atmospheric gravity waves (Arteru et al, 2005; Lognonne et al, 2006). In conjunction with this TEC research, improved techniques were developed to model the temporal development of the electron density distribution in the ionosphere (Occhipinti et al, 2006). While TEC inversion techniques yield very informative 3-D images of the perturbations, these are restricted to the regions possessing such networks and in general extend no more than 200 – 300 kilometres offshore.

The possible use of HF skywave radar as a seismometer emerged again in 2004 when the possible use of the French Nostradamus radar to monitor the ionospheric signatures of earthquake-generated Rayleigh waves was proposed (Occhipinti et al, 2004; Occhipinti et al, 2010). Although the spatial resolution of Nostradamus is not high, it shares with other HF skywave radars very high Doppler resolution which is the key to detecting small perturbations in the ionosphere. It was a natural step from this to consider the application of this radar to tsunami detection (Coisson et al, 2008), based on models of the generation and propagation of the AGW produced by the expanding tsunami waveform. Around the same time, a study by a German group (Marquardt, 2007) identified HF skywave radar as a candidate technology for the tsunami detection mission, while a comprehensive assessment of HF radar signature mechanisms was reported (Anderson, 2008).

This chapter presents an assessment of the performance of HF skywave radar in the role of a tsunami warning system, with reference to all the signature mechanisms identified in the cited literature. That is not to say that other signatures are absent – the scale and energy of tsunamis are such that it would be surprising if other possibilities did not exist. First, though, we describe the unusual properties of HF skywave radar.

2. General characteristics of HF skywave radar systems

Radars operating in the HF band (3 – 30 MHz) are distinctive in that they can exploit modes of electromagnetic wave propagation other than line-of-sight. Two modes in particular are commonly exploited – skywave propagation, which involves reflection from the ionosphere, and surface wave propagation, which refers to electromagnetic waves localised at the air-sea boundary and diffracted by the earth's curvature to illuminate the sea surface beyond the horizon. Radars exploiting the former mechanism are often referred to as over-the-horizon radars (OTHR) but as this description also fits radars employing the surface wave mode, it is preferable to use the terms 'skywave radar' and 'surface wave radar'. Both types are being

considered for tsunami warning (Anderson, 2008; Coisson et al, 2008; Barrick, 1979; Lipa et al, 2006; Heron et al, 2007; Dzvonkovskaya et al, 2009). Here we focus mainly on skywave radar, which can exploit tsunami signatures not accessible to surface wave radar; in addition it provides far greater spatial coverage.

The main physical differences between HF radars (of either variety mentioned) and the familiar microwave band radars result from the relative wavelengths. Whereas microwave frequencies correspond to wavelengths of 1 – 30 cm, HF frequencies equate to wavelengths of 10 – 100 m. As a consequence, antennas tend to be 10^2 — 10^3 times larger. Figure 2 shows the 2.8 kilometre receiving antenna array of the Jindalee skywave radar in Central Australia.

Fig. 2. Aerial view of the 2.8 km receiving array of the Australian Jindalee skywave radar, operational since 1982.

Representative values for some of the key radar parameters relevant to the tsunami warning mission are listed in Table 1. Although HF skywave radar is the subject of this chapter, HF surface wave radar parameter values have been included because such systems are much more common and have been widely promoted as tsunami sensing systems. A fairly comprehensive description of HF radars of both classes can be found in a recent survey (Headrick & Anderson, 2008b). Note that each of the Australian radars is essentially two radars, one a high power, high resolution system designed to detect aircraft and ships, the other a low power, low resolution system which provides frequency management advice (FMS). The latter has a significantly greater geographical coverage, as shown in Figure 1. For clarity, only one radar's FMS coverage is drawn.

Parameter	Typical values for HF skywave radar	Typical values for HF surface wave radar
total area within coverage (km^2) (subject to propagation availability)	~10^7	~10^5
range coverage (min→max) (km)	800 → 3500	5 → 180
angular coverage arc (deg)	90 – 360	60 – 180
angular beamwidth (deg)	0.3 – 3	3 – 12
resolution cell dimension (km)		
range	3 – 30	0.3 – 5
cross-range (at 2000 km)	10 – 100	n/a
number of spatial resolution cells monitored simultaneously		
range	20 – 250	30 – 250
beams	10 – 30	1 – 32
area observed simultaneously (km^2)	2×10^5	1×10^5
time taken for one observation (s)	16 – 64	50 – 300
unambiguous velocity band (ms^{-1})	± 20 – 50	± 10 – 30
effective velocity resolution (ms^{-1})	0.3 – 1	0.05 – 0.5

Table 1. Representative coverage and sampling properties of HF skywave radar when configured for tsunami detection. Optimum parameter choice varies with type of signature.

3. Tsunami signatures observable with HF skywave radar

3.1 Signature domains and mechanisms

The internal gravity wave-mediated ionospheric response is not the only tsunami signature which can be observed, at least in principle, by an HF skywave radar. In fact, it has been pointed out (Anderson, 2008) there are no fewer than six distinct mechanisms whereby tsunamis produce geophysical effects which could manifest themselves in HF skywave radar returns. It is relevant to point out that, of the identified mechanisms, HF surface wave radars observe only one – the advection, by the tsunami wave', of the shorter gravity waves which contribute most strongly to HF sea echo. Straightforward calculations reveal that a scheme for tsunami detection via the resulting Doppler shift is eminently feasible where the bathymetry is suitable (Barrick, 1979) and, after the Boxing Day tsunami, quite a number of HF surface wave radar groups conducted modelling studies of this approach (Lipa et al, 2006; Heron et al, 2007; Dzvonkovskaya et al, 2009). The other candidate tsunami signature domains identified as potentially amenable to detection by HF skywave radar are sea roughness modulation (Godin, 2004; Godin, 2008, Troitskaya & Ermakov, 2004), geomagnetohydrodynamic effects (Iyemori et al, 2005; Anderson, 2008) and infrasonic wave modulation of the lower ionosphere (Le Pichon et al, 2005; Koshevaya et al, 2004).

While it would seem that a considerable palette of potential tsunami signatures may be available, this diversity of opportunities is confronted by the realities of HF skywave radar operational performance. First, although the *potential* spatial coverage of HF skywave radar is commensurate with the perceived requirements of a tsunami monitoring system, not all of this vast region can be interrogated at any given time. The ionosphere, on which skywave propagation depends, experiences large variations over an extremely wide range of spatial

and temporal scales, so the surveillance volume which can be illuminated with adequate signal strength at any given time is only some fraction of the nominal coverage. Second, even if signal strength is adequate, most prospective tsunami signatures are degraded by fluctuations in the signal phase due to dynamical processes in the ionosphere. Third, HF skywave radar is vulnerable to interference and unwanted echoes which can obscure some of the desired signals. Fourth, some natural geophysical phenomena produce Doppler signatures which are locally indistinguishable from those expected from a tsunami, so the probability of false alarm could be high. It is for these reasons that we need to assess the prospective role of HF radar as a component of a tsunami warning system in terms of the statistics of availability of propagation meeting the specific threshold requirements of the tsunami signatures of interest, taking into account the likelihood of coincident events which could result in tsunami-like signatures.

The geophysical domains in which tsunamis 'write' a signature which is plausibly observable with HF radars of one form or another fall into three categories :

- changes to ocean surface geometry and dynamics
- changes to ionosphere geometry and dynamics
- phenomena associated with tsunami run-up and landfall

In order to predict and interpret HF radar signatures of tsunamis, we need a physical model for each mechanism.

3.2 Signatures involving scattering from the ocean surface

Scattering of HF radio waves from the time-varying ocean surface results in a complex phase modulation which manifests itself in the signals received by an HF radar as an imposed Doppler spectrum. The structure of this spectrum is determined by the spatio-temporal covariance function of the surface or, equivalently, by the distribution of surface gravity waves and currents in each resolution cell. The former are conventionally represented by the directional wave spectrum, spanning wavelengths in the range 10^0 — 10^2 m, the latter by a three-dimensional mean field associated with quasi-stationary large-scale flows. Both waves and currents are influenced by the passage of a tsunami, leading to distinct signatures as discussed below.

Signature 1 : The advection signature

Tsunamis are global scale phenomena, and hence a rigorous treatment requires the full Navier-Stokes equation on a rotating earth,

$$\rho\left[\frac{\partial v}{\partial t}+\left(\vec{v}\cdot\nabla\right)\vec{v}\right]=-\nabla p+\rho\vec{g}-\Omega\times\left(\Omega\times\vec{r}\right)-2\Omega\times\vec{v}+\frac{1}{3}\mu\left(\nabla\left(\nabla.\vec{v}\right)\right)+\mu\nabla^2\vec{v} \tag{1}$$

together with the general equation of continuity,

$$\frac{\partial\rho}{\partial t}+\left(\nabla\cdot\left(\rho\vec{v}\right)\right)=0 \tag{2}$$

and the associated boundary conditions. Nevertheless, many essential characteristics can be derived from a simplified model obtained by assuming incompressible, irrotational, inviscid flow, ignoring Coriolis and centrifugal effects, setting aside consideration of acoustic waves in the fluid, side-stepping the possibility of significant ambient currents and noting that the

wave amplitude will be small except in the immediate coastal zone. In this case, setting $\vec{v} = \nabla\varphi$, the Navier-Stokes equation reduces to the equation for potential flow:

$$\nabla_{xy}^2\varphi + \frac{\partial^2}{\partial z^2}\varphi = 0, \quad -h \le z \le \eta \tag{3}$$

which we can solve after imposing kinematic boundary conditions at the free surface and on the bottom, and the dynamic boundary condition at the free surface. As is well known, to first order, (1) reduces to

$$\frac{\partial^2}{\partial t^2}\varphi_1 + g\frac{\partial\varphi_1}{\partial z} = 0 \tag{4}$$

with solution

$$\begin{aligned} \eta_1 &= a\exp\left\{ i\left(\omega t + \vec{K}\cdot\vec{r}\right)\right\} \\ \varphi_1 &= \frac{iag}{\omega\cosh\left(Kh\right)}\exp\left\{ i\left(\omega t + \vec{K}\cdot\vec{r}\right)\right\}\cosh\left[\left|\vec{K}\right|\left(z+h\right)\right] \end{aligned} \tag{5}$$

Substituting in (4) yields the dispersion relation

$$\omega_1^2 = gK\tanh Kh \tag{6}$$

For tsunamis, where the wavelength is much greater than the depth, (6) reduces to

$$\omega_1 = K\sqrt{gh} \tag{7}$$

so the wave celerity is independent of wavelength and a function only of depth,

$$v = \frac{\omega}{\mathrm{K}} = \sqrt{gh} \tag{8}$$

A feature of the solution (5) is that as the depth parameter *Kh* decreases, the flow becomes increasingly horizontal, and essentially in phase throughout the water column. In the case of tsunamis, the fluid motions have horizontal length scales of the order of 10^5 m, the depth parameter is small (~ 0.25 for 4000 m depth) and vertical shear is negligible except near the sea floor. Consider now the effect on the short gravity waves which are responsible for HF sea clutter. The hydrodynamic modulation amplitude is of the same order as the ratio of current velocity to the wave group velocity in the reference frame of the current. In the deep ocean, this ratio is ~ 5×10^{-5} for tsunamis so the short surface gravity waves are advected uniformly by the bulk fluid motion as the tsunami progresses. The observed monostatic radar Doppler spectrum will have a frequency offset commensurate with the orbital velocity $\vec{u}$ of the tsunami wave. In the case of the two first-order Bragg lines which are dominant at HF, the large-scale spatial modulation of the Doppler shift is given by

$$\omega_d = 2\frac{F}{c}\left[\pm\sqrt{\frac{g}{K}} - \vec{k}\cdot\vec{u}\right] \tag{9}$$

Differentiating (5) and evaluating at the surface, the advection velocity field structure is given by

$$u(\vec{r}) = \frac{g\eta(\vec{r})}{\sqrt{gh}} \tag{10}$$

with maximum value

$$u_{\max} = \frac{ag}{v} \tag{11}$$

The Boxing Day tsunami achieved an amplitude of ~ 0.7 m over the deep ocean, while the celerity was ~ 200 m.s^{-1}. Substituting,

$$u_{\max} \approx 0.035\ m.s^{-1} \tag{12}$$

This is below the minimum current velocity that can be measured with HF radar under favorable conditions so, prima facie, skywave radar cannot detect the deep ocean Bragg scatter advection signature.

For a tsunami entering water of variable depth, in the absence of dissipation, conservation of energy requires that the wave amplitude increases as the wave slows,

$$energy\ flux = \frac{1}{2}\rho g v a^2 \propto h^{\frac{1}{2}} a^2 \tag{13}$$

implying that $a \propto \sqrt[4]{h}$. According to this relation, a tsunami of amplitude 0.7 m in 4000 m depth will arrive at the 100 m isobath with an amplitude of 1.75 m. Therefore, as the wave crosses the continental slope, the modulation will increase as the tsunami slows, first becoming evident as enhancement of the bulk transport of the surface gravity waves described above, then via progressively more nonlinear effects such as wave bunching and induced breaking.

Figure 3 shows the synthetic HF radar Doppler advection signature for a tsunami approaching a coastline with a bathymetric gradient of 10 metres per kilometre. The radar is set back 1200 km from the coast and a sporadic-E layer at 100 km altitude used to set the scattering geometry. The HF radar frequency is 15 MHz, with a 50 kHz bandwidth waveform corresponding to a range resolution of 3 km. The onshore wind speed used for this example is 5 ms^{-1}. It is clear that the advection is concentrated in the last 10 – 15 km from the shoreline, so warning time would be very limited, even allowing for the reduced tsunami speed. Moreover, ocean currents and mesoscale eddies have Doppler signatures with comparable shifts, so discrimination is nontrivial.

Signature 2. The surface roughness signature

The most immediate form of interaction is aerodynamic coupling with the adjacent neutral atmosphere. Conceptually, the progressive tsunami wave modifies the wind field above the surface, the modified wind field acts on the prevailing wave distribution, and this may cause a measurable change to its radar signature via the wind stress, given by

$$\vec{\tau} = \rho_{air} C_D \left| \vec{u}_{air} - \vec{u} \right| \cdot \left(\vec{u}_{air} - \vec{u} \right) \tag{14}$$

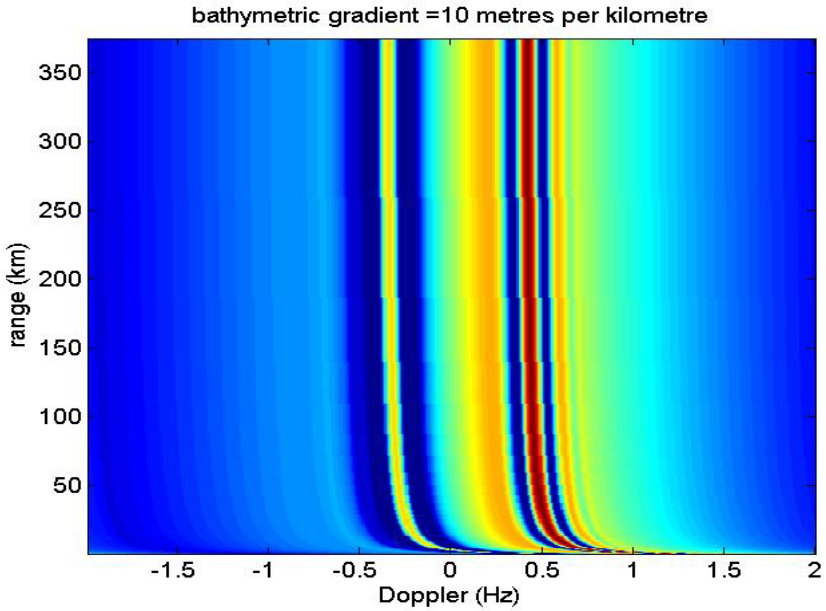

Fig. 3. A synthetic range-Doppler map for the case of a tsunami approaching a coastline with a bathymetric gradient of 10 metres per kilometre. The HF radar frequency is 15 MHz, with range resolution 3 km, and the onshore wind speed 5 ms^{-1}.

where ρ_{air} and $\vec{u}_{air}$ are the density and velocity of the air just above the surface, C_D is the drag coefficient and $\vec{u}$ is the water surface velocity given by (11). It was shown in the preceding section that the orbital velocity of the water particles at the surface is very small in deep water, of the order of a few centimetres per second. On ocean basin scales, $\left|\vec{u}_{air}\right|$ ~ 10 ms^{-1} so the tsunami-induced change in wind stress is ~ 0.7%, which is insignificant. Even in the equatorial region, where $\left|\vec{u}_{air}\right|$ ~ 1 ms^{-1}, the corresponding modification to the wind stress may reach ~ 7%, which is starting to appear promising. Unfortunately, in such calm conditions the horizontal scale length of surface conditions is generally low, wave development is equally variable, equilibrium seldom prevails and, as a consequence, the sea clutter Doppler spectrum is less informative.

Despite these arguments, so-called "tsunami shadows" have been reported, both visually and in microwave radar returns. This motivated a study to investigate the physics of atmosphere-ocean coupling using a more sophisticated argument (Godin, 2004; Godin, 2008). This analysis showed that, by parametrising the near-surface Reynolds stresses in terms of a turbulent viscosity which varies with height across the logarithmic boundary layer, the Navier-Stokes equation (1) can be reduced to an ODE taking the form

$$\begin{aligned}\frac{d}{dy}\left(\gamma^2\frac{dh}{dy}\right)-\kappa^4\alpha^2\gamma^2 h &= -4i\kappa^4\alpha^2\frac{d}{dy}\left[y\frac{d}{dy}(\gamma h)\right]\\ &+i\left(\frac{d^2}{dy^2}+\kappa^4\alpha^2\right)\left[\frac{y}{\gamma}\frac{d}{dy}\left(\gamma^2\frac{dh}{dy}\right)+\kappa^4\alpha^2\gamma y h\right]\end{aligned} \tag{15}$$

Under reasonable assumptions, this equation possesses wave solutions h_k, one class viscous, the other inviscid. Combining these to satisfy the boundary conditions on the surface yields expressions for the vertical and horizontal perturbations to the mean wind within the boundary layer:

$$v_H = u_0 \frac{\gamma(y)}{B_1\left(\beta^{-1},\beta^{-1}\right)}\left[B_1\left(\beta^{-1},y\right)+\frac{kD}{\kappa^2\alpha}B_2(y)\right]$$
$$v_V = iu\frac{\gamma(y)}{B_1\left(\beta^{-1},\beta^{-1}\right)}\left[\kappa^2\alpha B_3(y)-kDB_1\left(y,\beta^{-1}\right)\right] \quad (16)$$

where the B_k are known functions defined in terms of the h_k.
Analysis of these equations reveals that v_v is of the order of kDu_0, comparable with the vertical velocity of the water surface, a very small quantity. In contrast, the horizontal surface wind is driven much more strongly: v_H can be comparable with the unperturbed wind velocity, as illustrated in Figure 4.

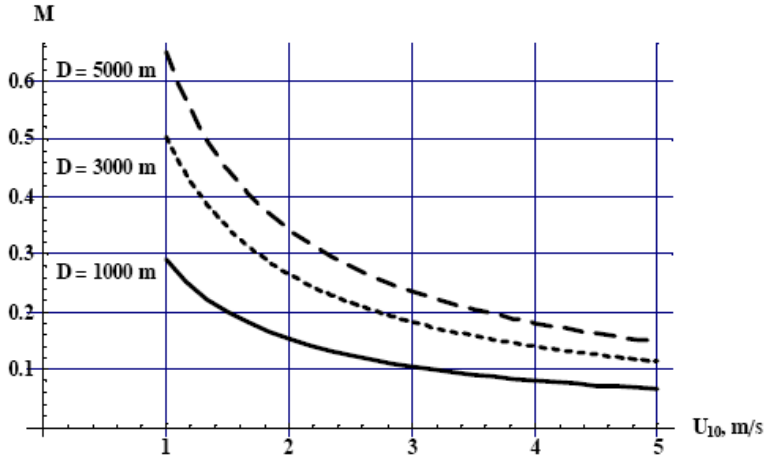

Fig. 4. Fractional change ξ in surface wind speed as a function of the unperturbed wind speed (Godin, 2008)

Under this model, the criterion for HF radar detectability should be gauged by comparing the spectrum computed for wind speed u with that computed for wind speed u′ given by

$$u' = \left(1 \pm \xi(u)\right)u \quad (17)$$

Figures 5 shows the predicted HF Doppler spectra for wind speeds u and u′ as defined in the text, for u = 4 ms^{-1}, for the case of an opposing orientation; the difference between the two is plotted in Figure 6. The corresponding plots for the aligned orientation are included as Figures 7 and 8. It can be seen that the difference is no longer negligible and may well be observable. This is not the case for higher prevailing wind speeds where the Doppler spectrum tends to saturate.

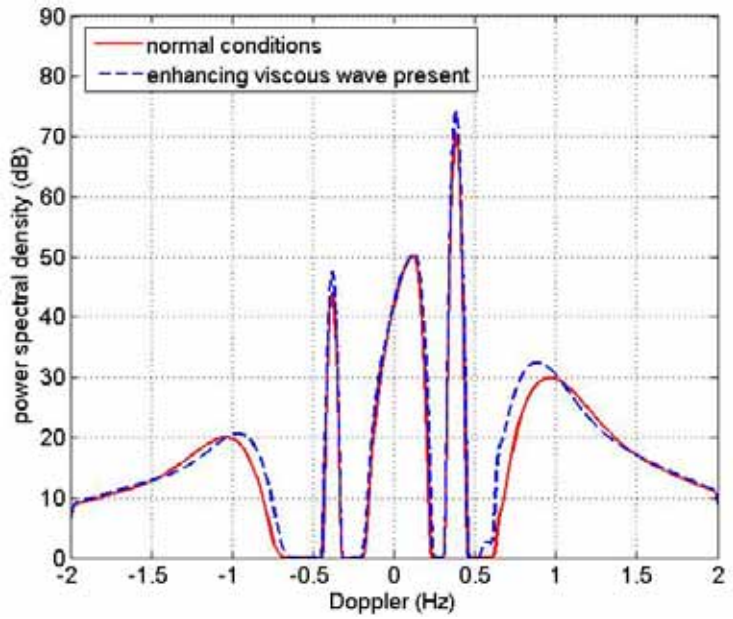

Fig. 5. Predicted HF sea clutter spectra for an ambient wind speed of 4 ms^{-1} with the viscous wave aligned with the ambient wind. Radar frequency 15 MHz

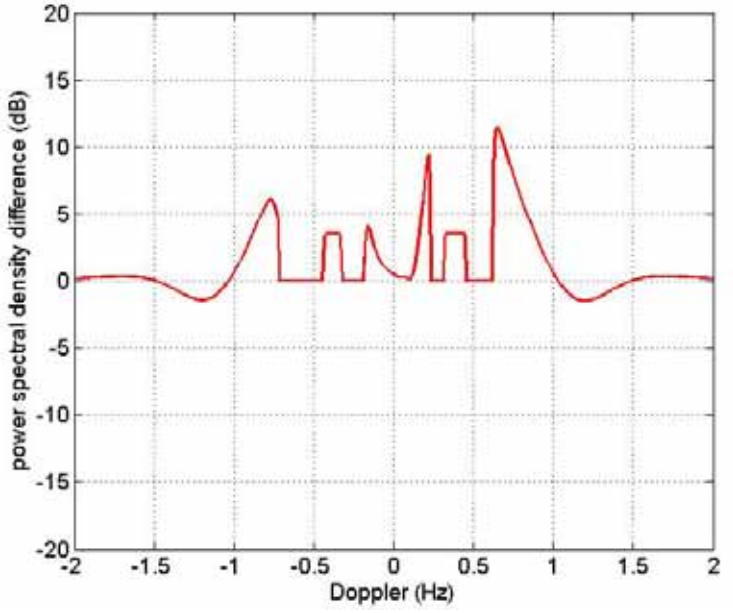

Fig. 6. The incremental change to the Doppler spectrum arising from the viscous wave for the aligned case.

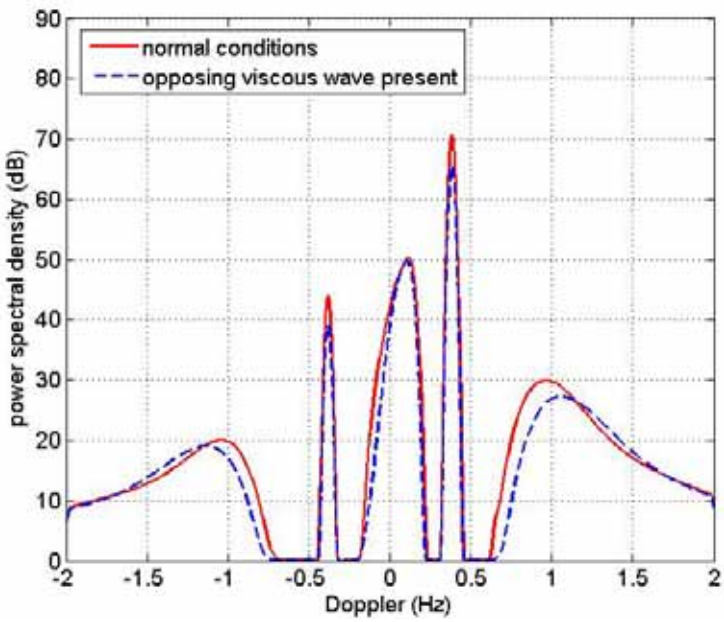

Fig. 7. Predicted HF sea clutter spectra for an ambient wind speed of 4 ms^{-1} with the viscous wave opposing the ambient wind. Radar frequency 15 MHz

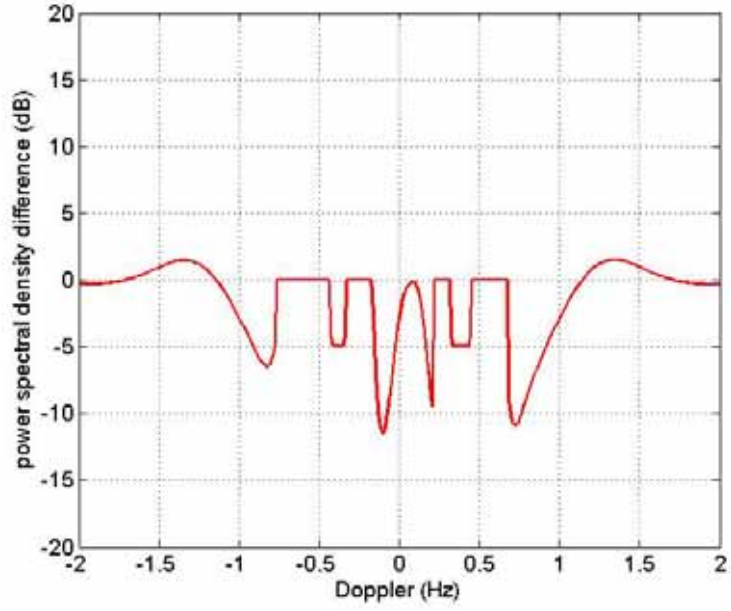

Fig. 8. The incremental change to the Doppler spectrum arising from the viscous wave for the opposing case

Experimental observations of changes to the sea roughness across the Boxing Day tsunami were made by the Jason-1 satellite at C- and Ku- bands (Troitskaya & Ermakov, 2006; Godin et al, 2009). Their swathe widths are well matched to measurement with HF radar, that is, a few tens of kilometres. Of course HF radar scattering mechanisms involve longer waves than those preferentially sampled by Jason-1, but the fact that changes were observed supports the viscous wave hypothesis.

3.2 Signatures involving the ionosphere

The ocean is coupled to the ionosphere by several physical and chemical processes of which two offer the prospect of generating a tsunami signature – mechanical coupling via the atmosphere and magnetic coupling via the geomagnetic field. The more obvious of these is the mechanical forcing due to the change in elevation of the water surface associated with the tsunami profile $\eta(\vec{x},t)$. As noted earlier, tsunami wavelengths are much greater than the water depth so the normal wave modes are essentially non-dispersive and the profile is, to first order, unchanging as the tsunami progresses, so it can be written as $\eta(\vec{x}-\vec{v}t)$ where $\vec{v}$ is the tsunami velocity. The shape of the profile is governed by the nature of the seismic displacement. It follows that the lower boundary of the atmosphere is subjected to a spatially and temporally varying forcing so the Navier-Stokes equation takes the form

$$\rho\left[\frac{\partial v}{\partial t}+(\vec{v}\cdot\nabla)\vec{v}\right]=-\nabla p+\rho\vec{g}+F \tag{18}$$

where the forcing terms correspond to compressibility, buoyancy and tsunami forcing respectively. An expression for F follows from considering the moving tsunami profile as a generalised piston, which performs work on the atmosphere according to the relation

$$\frac{\delta W}{\delta t}=-P_0\nabla\eta(\vec{x}-\vec{v}t)\cdot(\vec{v}-\vec{u}) \tag{19}$$

where P_0 is the atmospheric pressure at sea level and $\vec{u}$ is the wind velocity.

In the absence of external (tsunami) forcing, the Navier-Stokes equation, together with the equation of continuity,

$$\frac{\partial\rho}{\partial t}+\left(\nabla\cdot(\rho\vec{v})\right)=0 \tag{20}$$

and the equation of state for adiabatic behaviour,

$$\frac{\partial p}{\partial t}+\vec{v}\cdot\nabla\rho-C_0^2\left[\frac{\partial\rho}{\partial t}+\vec{v}\cdot\nabla\rho\right]=0 \tag{21}$$

describes the characteristic modes of the neutral stratified atmosphere (Hines, 1960). Here C_0 is the speed of sound,

$$C_0^2=\frac{\gamma p}{\rho} \tag{22}$$

Letting Ψ denote the vector of normalised perturbations of density and pressure from their mean values, together with the horizontal and vertical components of the fluid velocity vector,

$$\vec{\Psi} = \begin{bmatrix} \rho'/\rho_0 \\ p'/p_0 \\ v_z \\ v_x \end{bmatrix} \tag{23}$$

and setting $H = -\rho_0 . \left(\frac{\partial \rho_0}{\partial z} \right)^{-1}$, the scale height,

we have

$$\begin{vmatrix} i\omega & 0 & -ik_x & -1/H - ik_z \\ 0 & -ik_x C_0^2/\gamma & i\omega & 0 \\ g & -C_0^2(1/H + ik_z)/\gamma & 0 & i\omega \\ -i\omega C_0^2 & i\omega C_0^2/\gamma & 0 & (\gamma - 1)g \end{vmatrix} \cdot \vec{\Psi} = 0 \tag{24}$$

whence we obtain

$$\omega^4 - \omega^2 C_0^2 \left(k_x^2 + k_z^2 \right) + (\gamma - 1) g^2 k_x^2 + i\gamma g \omega^2 k_z = 0 \tag{25}$$

that is, the dispersion relation for atmospheric waves. For an upward propagating wave we require that

$$k_z = k_z^{'} + i\frac{\gamma g}{2C_0^2} = k_z^{'} + i\frac{1}{2H} \tag{26}$$

We can then rewrite the dispersion relation as

$$\omega^2 C_0^2 k_z^{'} = \omega^4 - \omega^2 \left(C_0^2 k_x^2 + \frac{\gamma^2 g^2}{4C_0^2} \right) + (\gamma - 1) g^2 k_x^2 \tag{27}$$

For a given horizontal wavenumber k_x, a real solution for $k_z^{'}$ exists only when the right hand side of ( ) is non-negative. The roots of the quadratic obtained by setting it to zero, ω_1 and ω_2, divide the frequency domain into three bands of possible wave solutions:

i. $\omega < \omega_1 < \sqrt{(\gamma - 1)} \frac{g}{C_0} \equiv \omega_b$

This band corresponds to internal gravity waves, driven by buoyancy forces; ω_b is the Brunt-Vaisala frequency.

ii. $\omega > \omega_2 > \frac{\gamma g}{2C_0} \equiv \omega_a$

This band corresponds to acoustic waves, driven by compressibility forces; ω_a is the acoustic cut-off frequency.

iii. $\omega_1 < \omega < \omega_2$

This band corresponds to Lamb waves, which propagate only in the horizontal direction with $k_z^{'}$ purely imaginary.

In the lower atmosphere, $\frac{\omega_b}{2\pi} \sim 2.9 \times 10^{-3}$ Hz while $\frac{\omega_a}{2\pi} \sim 3.3 \times 10^{-3}$ Hz. At 400 km altitude these become 9.5×10^{-4} Hz and 1.1×10^{-3} Hz respectively.

From the viewpoint of tsunami detection, the most important property of these atmospheric waves is the amplification of the disturbance produced as they rise and the air density decreases. In the absence of attenuation, conservation of energy dictates that the amplitude of the vertical displacement is proportional to $\rho_0^{-1/2}(z)$. Thus, between sea level and an altitude of 125 km, the density decreases by a factor 10^{-8} so the wave amplitude grows by 10^4. A tsunami-induced surface displacement of amplitude of 10 cm may generate a displacement of ~1 km in the lower E-region. For F-region heights, the idealised amplification factor becomes 10^5 but by this height, kinematic viscosity exerts considerable damping, with peak displacement occurring at ~ 300 km. The collisional interaction of the neutral gas species with the ionised components leads to the perturbations in electron density which manifest themselves as travelling ionospheric disturbances, and it is these which have been proposed by various researchers as a possible tsunami signature. Particular interest has been shown in the three-dimensional imaging of the electron density distribution via tomographic processing of total electron content data. The time development of ionospheric perturbations over Japan, extracted from the GEONET satellite network, was found to correlate extremely well with a tsunami originating near Peru (Artru et al, 2005; Lognonne et al, 2006), and further support for the concept of TEC imaging of tsunami-generated ionospheric disturbances has come from modelling of those induced by the 2004 Boxing Day tsunami (Occhipinti et al, 2006).

The strength of the coupling between the time-varying surface displacement and any particular atmospheric wave component depends on a number of factors including not only the amplitude of the displacement but, just as importantly, its waveform. In principle this consists of both the forcing seafloor Rayleigh wave as mapped to the water surface and the freely-propagating hydrodynamic response, that is, the tsunami (Yamashita & Sato, 1976). The actual response of the neutral atmosphere at ionospheric heights to a particular tsunami event may be estimated by integration over the tsunami profile using an appropriate Green's function for the propagator in the stratified atmosphere. Various approximations to the Greens' function have been reported (Francis, 1974). Equivalently, one can employ a modal expansion in terms of the characteristic inertial-gravity and acoustic wave modes, matching the boundary conditions at the surface. The associated response of the electron density distribution in the ionospheric plasma involves an additional term in the equation of motion to account for the electromagnetic effects,

$$\rho\left[\frac{\partial v}{\partial t} + (\vec{v}\cdot\nabla)\vec{v}\right] = -\nabla p + \rho\vec{g} + \vec{j}\times\vec{B}_0 \tag{28}$$

where $\vec{j}$ depends on the Pedersen, Hall and parallel conductivities in the geomagnetic field, so the response sensed by HF radio waves is both location and direction dependent. The inclusion of Coriolis effects adds yet more complexity to the formulation. While these

phenomena demand attention for a full parametric description, here we are concerned only with the broad issues of measurement by HF skywave radar.
An important consideration with the internal gravity wave disturbance is that it propagates obliquely upwards not at the acoustic velocity but at a much lower speed. As a consequence, the energy injected by the tsunami into the atmosphere will take 1 – 2 hours to reach the ionosphere where it can produce ionospheric effects detectable by an HF radar. The time taken is influenced by the ratio of the vertical and horizontal wavelengths, which in turn are governed by the tsunami parameters

Signature 3. The ground clutter Doppler spectrum modulation signature

When the internal gravity wave reaches the ionosphere, it perturbs the electron density distribution, predominantly via ion-neutral collisions and the Lorentz force. HF radar signals reflected from the perturbed ionosphere are modulated by the disturbance and this is manifested in the Doppler spectrum of ground clutter observed via the skywave path. Figure 9 presents a 'snapshot' of the Doppler shift associated with an unusual monocycle disturbance which was tracked by the Jindalee radar for over two hours, during which it changed form only slightly. Propagating towards the equator, the front half-cycle showed a

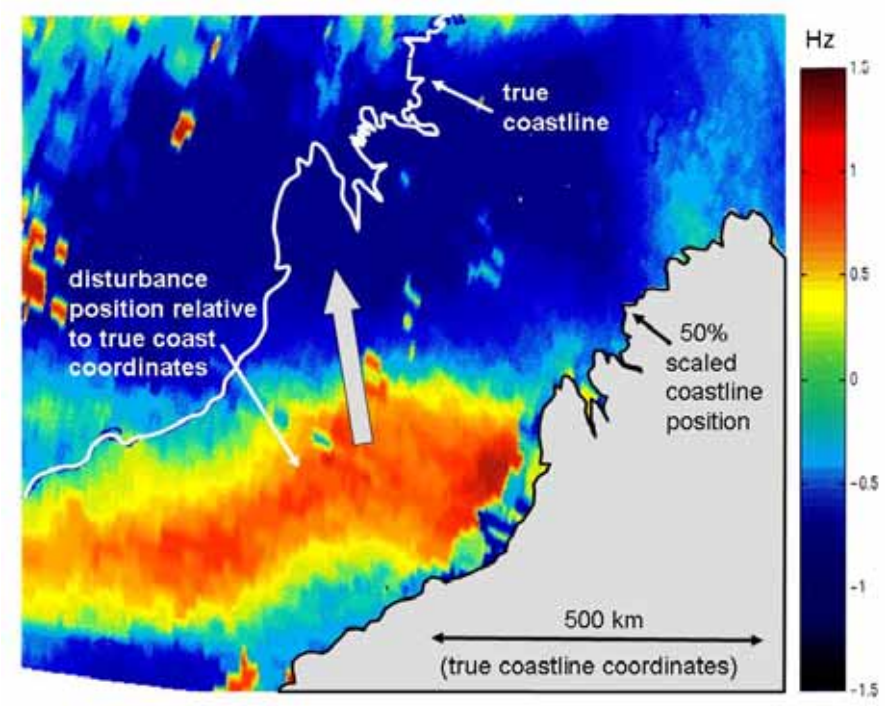

Fig. 9. A large-scale disturbance mapped with the Jindalee radar in 1986. The Doppler shift was measured for skywave paths to the ocean surface off NW Australia, then the resulting radar data geographically re-positioned so that the path Doppler shifts lie not at the corresponding ground reflection points but at the mid-points (control points) of the ray trajectories, where the phase modulation due to the disturbance is concentrated

significant negative Doppler shift, consistent with the ionosphere being displaced upwards by a gravity wave, followed by a positive Doppler restoring phase. The origin of this disturbance is not known, but it is included here because it resembles what we might expect from a tsunami.

Signature 4. The ground clutter intensity modulation signature

In addition to modulating the signal phase and hence imposing a Doppler shift on the radar echoes, internal gravity waves distort the virtual height distribution over the affected area, effectively producing a curved reflecting layer in the ionosphere. This results in focusing and defocusing of the radar signals, manifesting itself on the radar displays as a strong intensity modulation of the ground clutter. A good example of this is shown in Figure 10, a backscatter ionogram recorded with the Jindalee radar. Several cycles of a quasi-periodic disturbance are clearly visible.

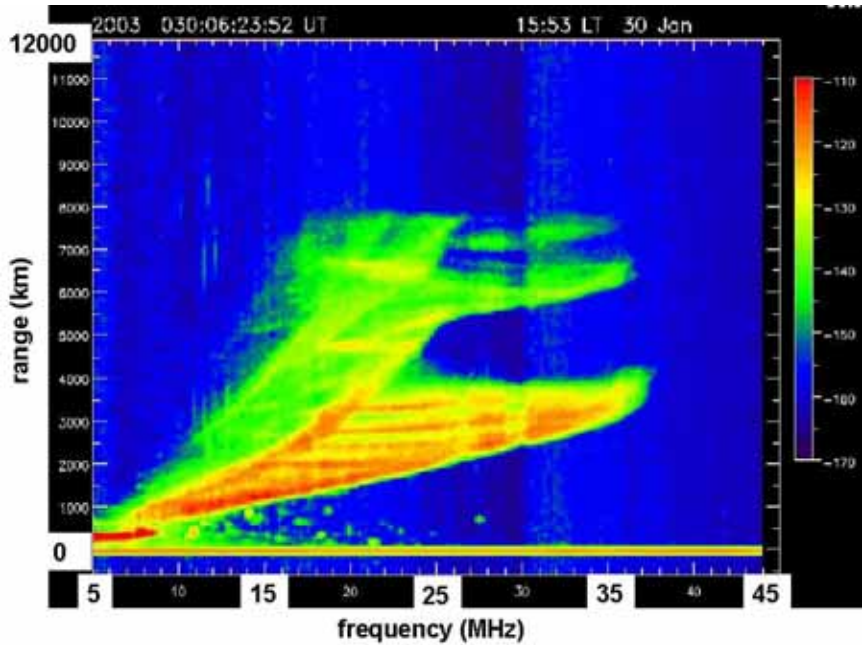

Fig. 10. A backscatter ionogram recorded during the passage of an internal gravity wave packet with 4 or 5 cycles. The bands of focusing and defocusing are almost independent of sounding frequency, supporting the interpretation. The fringe spacing is 470 km

Signature 5. The infrasonic ionosphere modulation signature

As noted above, the dispersion relation admits compression-dominated acoustic modes as well as buoyancy-dominated internal gravity waves, so there is a priori some prospect that these too might modulate the ionosphere in a way which impacts on HF radar signals. On closer examination, though, the outlook is not hopeful. At ionospheric heights, kinematic viscosity increases rapidly and this effectively imposes a low-pass filter on the wave (Spitsyn & Taraschuk, 1994). Figure 11 (adapted from Najita et al, 1974), shows the combined effect of amplitude growth and viscosity versus acoustic frequency, as a function

of altitude. Clearly the spectrum of the tsunami-generated infrasonic emissions will govern its influence on a given HF skywave signal path because the fan of rays representing skywave radar illumination at a given frequency leaves substantial regions of the ionosphere unsampled. A second consideration is the likely radiation pattern of the emissions : over land, Rayleigh earthquake waves propagate at a speed much higher than the acoustic velocity C, so the source is horizontally in phase and effective upward radiation is achieved; moreover, this will be augmented by refractive focussing in stable atmospheric conditions. Over the ocean, the tsunami speed is typically ~ $0.7C_0$ so one might expect infrasonic waves excited by a tsunami to be radiated preferentially at a depth-related angle,

$$\theta_{eff} = \frac{\pi}{2} - ar\cos\left(\frac{C}{\sqrt{gD}}\right) \tag{29}$$

which corresponds to ~ 53° in water of depth 4000 m. Apart from the obvious signal loss due to increased atmospheric absorption along oblique paths, refractive signal trapping in the presence of atmospheric temperature inversions will be exacerbated.

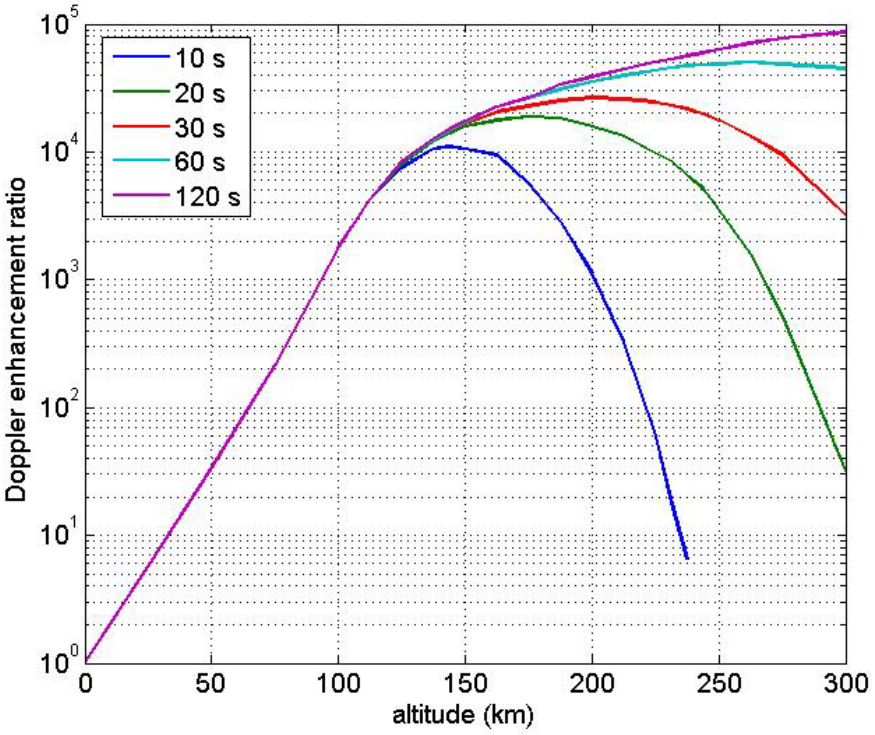

Fig. 11. The ratio of effective particle displacement at altitude to the displacement at sea level taking into account kinematic viscosity and density profiles.

In addition to these considerations, there is the issue of the coupling mechanism. Under 'frozen-in' field conditions, as apply in the ionosphere, infrasonic frequencies excite ULF

magnetohydrodynamic (MHD) disturbances, that is, Alfven and fast mode oscillations at low latitudes and field line resonances at higher latitudes. These phenomena modulate the phase of HF radio waves via three mechanisms (Sutcliffe & Poole, 1976), namely, magnetic field changes, advection of the bulk plasma and compression of the plasma. There is also the issue of microbaroms, infrasonic radiation from standing waves in the ocean at long swell frequencies, though potentially these may be separable in the frequency domain.
On the other side of the ledger, infrasonic waves propagate to the lower ionosphere in about 10 minutes, in contrast to internal gravity waves which may take up to 150 minutes to reach the same height. Further, HF skywave radar has shown a remarkable ability to extract ULF phase modulations from ground and sea backscatter (Anderson & Abramovich, 1998). It should be helpful for discrimination that the azimuthal wavenumbers of ULF waves of magnetospheric origin are observed to be low, whereas tsunami-generated ULF disturbances are likely to be much more localised. Once the phase modulation sequence has been estimated, information about the cause may be inferred from the geographical distribution of the sequence structure and its temporal evolution. That this discrimination is possible can be seen from Figure 12 which shows the demodulation sequences of two specific ionospheric perturbations. Figure 12a shows the sequences for 4 range cells separated by 50 km, that is, every tenth range cell in the particular radar dwell.

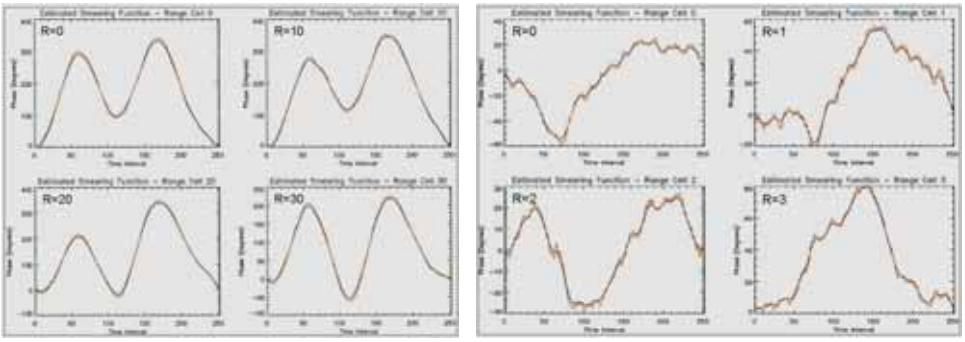

(a) (b)

Fig. 12. (a) Demodulation sequences for every 10th range cell for the case of an internal gravity wave; (b) demodulation sequences for adjacent range cells during a transient event of unknown origin. Data obtained with the Jindalee radar

The demodulation sequences are almost identical, indicating the high spatial coherence of the ionospheric perturbation which was identified by other means as a travelling ionospheric disturbance, that is, a manifestation of an internal gravity wave. In contrast, Figure 12b shows the behaviour observed during a different event; in this case the 4 range cells chosen were consecutive in range, a mere 5 km spacing, yet the sequences are far less correlated. This event was not formally identified with any particular cause.

Signature 6. The geo-magnetohydrodynamic tsunami-ionosphere coupling signature

The magnetic field within the terrestrial environment is the sum of contributions from a number of sources : (i) dynamo currents within the earth's core, (ii) magnetised rocks and other material in the earth's crust, (iii) electric currents in the ionosphere, and (iv) electric currents produced by the sea water motions. The last of these has recently been proposed as

a candidate mechanism for tsunami detection and measurement (Anderson, 2008). Typically (ii) and (iii) contribute an amount less than 1% of the primary geomagnetic field due to (i), so they can often be neglected. The term of interest, (iv), is much smaller again in the case of normal ocean waves and swell but for tsunamis, with representative length scales some 10^3 times greater, a commensurate gain in the generated field perturbation might be expected. An attractive feature of this mechanism, if it is observable, is that such a disturbance propagates at the speed of light below the ionosphere.

Magnetic disturbances in the ionosphere are routinely observed with HF skywave radar when those disturbances come from above, that is, from the magnetosphere. The question addressed here is whether or not tsunamis might produce a detectable ionospheric signature from below. The mechanism involves the propagation to ionospheric heights of the magnetic field disturbances generated within the ocean body; there they can manifest themselves as Alfven waves which, under the prevailing 'frozen-in' field conditions, modulate the electron density distribution and hence impose a phase modulation on transiting radiowaves, very much as the infrasonic waves discussed earlier. Unlike the latter, though, there is little impediment to the disturbance propagating to F-region heights.

Evidence for this kind of geo-magnetohydrodynamic tsunami-ionosphere coupling appears to be available from some magnetometer records (Iyemori et al, 2005). Of course, the key limitation via-a vis tsunami warning would be discrimination of such effects from the background of similar disturbances arising from other mechanisms.

To develop a model for these effects, we need to augment the hydrodynamic equations of earlier sections with Maxwell's equations. Noting that the background geomagnetic field may be taken as uniform over a tsunami wavelength, we can write the total field as

$$\vec{B} = \vec{B}_{geo} + \vec{b} \tag{30}$$

where, given that $\left|\vec{b}\right| << \left|\vec{B}_{geo}\right|$ the conduction current is given by $\vec{J} = \sigma(\vec{E} + \vec{v} \times \vec{B}_{geo})$

Here $\vec{E}$ is the electric field in a stationary frame of reference, $\vec{v} \times \vec{B}_{geo}$ is the motion-induced field and σ is the electrical conductivity of seawater, taken here as 4 mhos.m^{-1}. From Maxwell's equations,

$$\nabla \times \vec{b} = \mu_0 \vec{J} + \varepsilon\mu_0 \frac{\partial E}{\partial t} \tag{31}$$

but at tsunami wave frequencies, the displacement current in seawater is negligible, so the magnetic field perturbation $\vec{b}$ caused by the current is given simply by Ampere's law,

$$\nabla \times \vec{b} = \mu_0 \vec{J} \tag{32}$$

Further, the electric and magnetic fields are related by Faraday's law,

$$\nabla \times \vec{E} = -\frac{\partial \vec{b}}{\partial t} \tag{33}$$

The modest conductivity of sea water is essentially ionic, and hence the Lorentz body force on the fluid parcels is negligible compared with the pressure and buoyancy forces, so there are no hydromagnetic forces to be taken into account.

Taking the curl of (31), substituting for E from (33) and using the identity $\nabla\times\left(\nabla\times\vec{b}\right)=\nabla\left(\nabla\cdot\vec{b}\right)-\nabla^2\vec{b}$, we have

$$-\nabla^2 b=\sigma_0\left(-\frac{\partial\vec{b}}{\partial t}+\nabla\times\left(\vec{v}\times\vec{B}_{geo}\right)\right)-\varepsilon\frac{\partial^2\vec{b}}{\partial t^2} \tag{34}$$

where, from Section II, the fluid velocity associated with the tsunami, as modelled by a harmonic shallow water wave, is given by

$$\vec{v}\equiv\begin{bmatrix}v_x\\v_y\\v_z\end{bmatrix}=\begin{bmatrix}\dfrac{-ag\cosh\left(K\left(z+h\right)\right)}{\cosh\left(Kh\right)}\cos\left(K\left(x-ct\right)\right)\\0\\\dfrac{ag\sinh\left(K\left(z+h\right)\right)}{\cosh\left(Kh\right)}\sin\left(K\left(x-ct\right)\right)\end{bmatrix} \tag{35}$$

Inserting (35) into (34) yields a linear PDE which can be solved directly by Fourier transform. Thus we have a numerical model for the magnetic field perturbation caused by the tsunami. For normal sea waves, the field decays fairly rapidly above the surface with a decay factor related to the water wavelength. Given the relative length scales of tsunamis and wind waves, we may expect a tsunami to generate in-phase contributions up to the height of the ionosphere.

3.3 Signatures involving coastal processes

The arrival of a tsunami at a coastline will generate transient responses in some, though not all, of the signatures mentioned so far. These could be difficult to interpret but may not be hard to detect. Depending on the bathymetry, the advection signature will shift in Doppler before broadening as spatial refraction inhomogeneity and nonlinear wave development distort the near-unidirectional, non-dispersive deep water waveform prior to it breaking close to the shore. Prevailing current patterns will be disturbed on large and small scales (Reddy et al, 2009). Strong fixed scatterers on the shore may have their radar cross section changed drastically. Infrasound generation may be intensified, first because as the water depth decreases and the wave grows, large quantities of surface air are being compressed and rarefied, producing infrasonic waves of the observed frequency, around 0.03 Hz. A second mechanism is the interaction of the tsunami wave with the shoreline and regions of steep bathymetry(Yeh et al, 1994). Standing waves set up by reflection constitute an acoustic 'oscillator', similar to that responsible for microbaroms.

The relevance of all this to tsunami warning arises when a landmass engendering these transient responses lies closer to the source than the region to be alerted. In effect the landmass serves as a 'canary' inserted into the tsunami's near field to produce an amplified reaction. Thus it was reported that atmospherically ducted infrasonic radiation measured at monitoring stations in the Indian Ocean region two or three hours after the Boxing Day tsunami was highly correlated with the tsunami wave landfall on the coasts of Burma and Bangladesh (Le Pichon et al, 2005). Contingent on the presence of suitable islands or other

landmasses in the source region, this kind of sampling should not be overlooked. At the very least, opportunities to observe magnified advection signatures, as illustrated in Figure 3, should be exploited.

4. Limits to the performance of HF skywave radars in the tsunami warning role

The ability of HF skywave radar to detect and quantify any of the signatures discussed above is heavily constrained by factors such as (i) radar design, (ii) radar siting relative to the geographical area of concern, (iii) the instantaneous, diurnal, seasonal and inter-annual properties of the ionosphere insofar as it influences the skywave propagation channel, and (iv) the existence and prevalence of other geophysical phenomena whose signatures resemble those associated with tsunamis. Some of these issues have already been mentioned, many others are obvious. The severity of these limiting factors has often been under-estimated by those without direct experience with HF skywave radar systems, so it is apposite to provide some quantitative guide to what is achievable in practice, though leaving aside radar system issues.

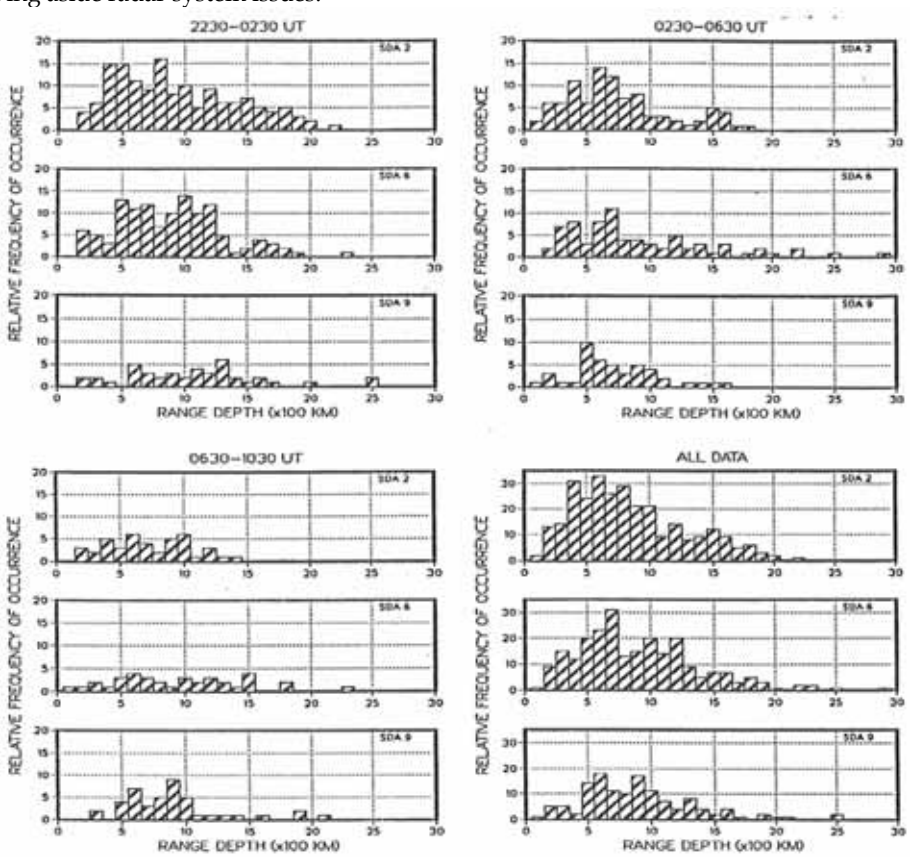

Fig. 13. Statistics of data quality relevant to observability of different tsunami signatures

First, with regard to skywave propagation, Figure 13 shows some statistics of data quality as measured on the SDA scale (Anderson, 1992). Here a rating of 9 represents near-perfect conditions, with no discernible Doppler shift, spectral broadening or multimode, whereas a rating of 0 applies to data with very low sub-clutter visibility and highly unstable phase paths. The data is binned according to instantaneous range coverage at the optimum frequency. The data used for this analysis is particularly realistic in the sense that it is not extracted from historical synoptic databases derived from frequency management systems but, instead, from records of specific missions undertaken by the Jindalee radar when the radar operators were doing their best to optimise the radar in real-time. Three levels of SDA index have been chosen for presentation here: 9, 6 and 2. At SDA=9, even the subtle roughness signature (Signature 2) should be readily observable and measurable, while at SDA=6, that would not be the case, though most ionospheric gravity wave signatures should be reasonably accurately measured. At SDA=2, large-scale ionospheric perturbations would be detectable on most occasions but would not be measurable with the accuracy needed to quantify tsunami parameters. Three time intervals have been selected : 0800 – 1200 local time, 1200 – 1600 local time and 1600 – 2000 local time. By and large, conditions at night are less favourable for the tsunami warning mission.

Figure 14, showing typical ionospheric activity as manifested in the Doppler domain, illustrates the challenge of discrimination between natural fluctuations and tsunami-generated disturbances. It seems likely that reliable discrimination will demand the use of physical models of the latter.

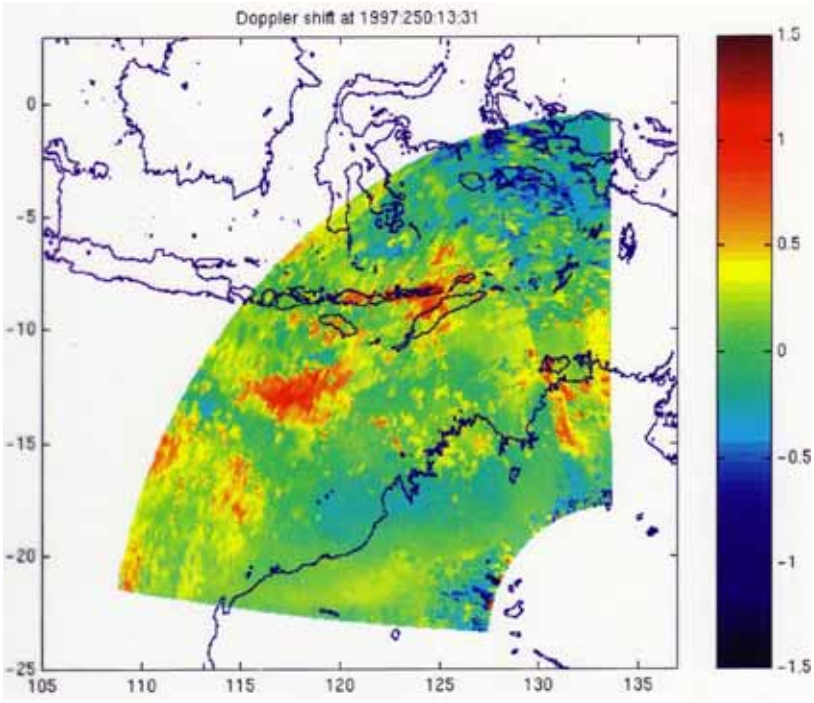

Fig. 14. A snapshot of the Doppler shift imposed on HF skywave backscatter signals under typical propagation conditions.

While detailed modelling of the physics of the signatures postulated above has yet to reach maturity, it is evident that the spatial and temporal scales of most of the identified phenomena are within the corresponding sampling resolution of HF skywave radar, while the radar Doppler resolution is exceptionally fine and likely to be the key to quantitative characterisation of tsunami amplitude. The utility of the various signatures in terms of warning and characterisation is far from uniform, as seen from the latencies listed in Table 2.

5. Conclusion

The survey reported here confirms that tsunamis may register signatures on HF radar systems via a number of different geophysical mechanisms. The mechanism cited frequently in the literature for the case of HF surface wave radar – that of advection of Bragg-resonant waves by tsunami-generated flows on the coastal shelf – is perhaps the most direct and the most accessible, but provides a useful warning only where the coastal shelf is sufficiently broad. Some other mechanisms may yield measurable signatures over much wider expanses of the ocean, though experience has shown that radar performance for this kind of diagnosis drops sharply beyond the one-hop zone.

CLASS	**PHYSICAL PHENOMENON**	**LATENCY (min)**	**VIABILITY FOR SKYWAVE RADAR**
1	Bragg-resonant gravity wave advection	1 - 2	Difficult via skywave Only possible on continental shelf
2	Viscous wave effects on surface roughness	30 – 100	Not yet demonstrated Latency an issue
3	Ionospheric disturbance caused by internal gravity waves	75 – 150	Detection well established Inversion yet to be demonstrated Poor latency Somewhat sensitive to geometry
4	Ionospheric disturbance caused by infrasonic waves	7 – 15	Limited effect Sensitive to geometry
5	Modulation of geomagnetic field by tsunami flows	1 – 2	Magnitude of effect not established Other causes exist Sensitive to geometry
6	Anomalous echoes from distant coastlines	150 – 200	Many variables Excessive latency Alternative explanations

Table 2. Summary of alternative signature latency and feasibility

While there can be no doubt that the reaction of the geophysical environment to the passage of a tsunami produces a number of effects which are potentially measurable with HF skywave radar, practical issues such as latency and false alarm rate are important considerations. There is also the matter of time line access – most if not all operational HF skywave radars have heavy operational tasking which cannot co-exist with a synoptic scale tsunami watch mission. The suitability of HF skywave radar as a tsunami sensor has been assessed here by examining the alternative mechanisms in enough detail to give some understanding of the physics involved, and interpreting modelled signatures in the context

of genuine operational radar performance statistics. The evidence seems unequivocal – more often than not, the signal quality of HF skywave radar echoes will not support the identification and interpretation of the more subtle tsunami signatures, even when parametric signature models achieve higher fidelity than prevails today. Given the nature and magnitude of the candidate signatures, and the variety of alternative causative mechanisms, the outlook can scarcely be regarded as promising, but neither does it rule out a possible contribution of HF skywave radar to a tsunami warning system.

6. References

Anderson, S.J. (1992). Adaptive Remote Sensing with HF Skywave Radar, Proceedings of the IEE, Part F, Vol.139, No.2, 182-192

Anderson, S.J. (1994). Tsunami detection with HF radar. *Proceedings of National Tsunami Workshop* 1994, Brisbane, Bureau of Meteorology

Anderson, S.J. & Abramovich, Y.I. (1998). A unified approach to detection, classification and correction of ionospheric distortion in HF skywave radar systems. *Radio Science*, Vol.33, No.4, 1055–1067

Anderson, S.J. (2008). Prospects for tsunami detection and characterisation with HF skywave radar. *Proceedings of the IEEE International Radar Conference*, Adelaide, September 2004

Arteru, J., Ducic, V., Kanamori, H. & Lognonne, P. (2005). Ionospheric detection of gravity waves induced by tsunamis. *Geophysics Journal International*, Vol. 160, 840-848

Barrick, D.E. (1979). A coastal radar system for tsunami warning, *Remote Sensing of Environment*, Vol. 8, 353-358

Coisson, P., Occipinti, G., Rolland, L., Lognonne, P. and Harmel, T. (2008). Can OTH radar help tsunami warning systems ? *Proceedings of the AGU 2008 Fall meeting*, San Francisco, December 2008

Dzvonkovskaya, A. & Gurgel, K.-W. (2009). Future Contribution of HF Radar WERA to Tsunami Early Warning Systems. *European Journal of Navigation*, Vol. 7, No. 2, 17-23

Francis, S.H. (1975). Global propagation of atmospheric gravity waves : a review. Journal of Atmospheric and terrestrial Physics, Vol.37, 1011-1054

Godin, O.A. (2004). Air-sea interaction and feasibility of tsunami detection in the open ocean. *Journal of Geophysical Research*, Vol. 109, C05002

Godin, O.A. (2008). Wind over fast waves and feasibility of early tsunami detection from space. *private communication*

Godin, O.A., Irisov, V.G., Leben, R.R., Hamlington, B.D. and Wick, G.A. (2009). Variations in sea roughness induced by the 2004 Sumatra-Andaman earthquake. *Natural Hazards Earth Systems Science*, Vol.9, 1135-1147

Headrick, J.M. & Anderson, S.J. (2008). HF Over-the-Horizon Radar. *Chapter 20, Radar Handbook*, Merrill Skolnik, (Ed.), 3rd edition, McGraw Hill

Heron, M.L., Prytz, A., Heron, S.F., Helzel, T. & Schlick,T.(2007). *Application of HF coastal ocean radar to tsunami observations.*

http://www.helzel.com/helzelmed/literature/Tsunami-Australia-6912.pdf

Hines, C.O. (1960). Internal atmospheric gravity waves at ionospheric heights. *Canadian Journal of Physics*, Vol.38, 1441-1481

Hines, C. O. (1972). Gravity waves in the atmosphere. *Nature*, Vol. 239, 73– 78

Iyemori, T., Nose, M., Han, D., Gao, Y., Hashizume, M., Choosakul, N., Shinagawa, H., Tanaka, Y., Utsugi, M., Saito, A., McCreadie, H., Odagi, Y. & Yang, F. (2005).

Geomagnetic pulsations caused by the Sumatra earthquake on December 26 2004. *Geophysical Research Letters*, Vol. 32, L20807,

Kinsman, B. (1967). *Wind Waves: Their Generation and Propagation on the Ocean Surface*, Prentice-Hall, Englewood Cliffs, NJ

Koshevaya, S.V., Grimalsky, V.V., Siqueiros-Alatorre, J., Perez-Enriquez, R. and Kotsarenko, A.N. (2004). Acoustic and acousto-gravity wave pulses caused by sources of seismic origin. *Physica Scripta*, Vol.70, 72-78

Le Pichon, A., Herry, P., Mialle, P. & Verguoz, J., Brachet, N., Garces, M., Drob, D. & Ceranna, L. (2005). Infrasound associated with 2004-2005 large Sumatra earthquakes and tsunami. *Geophysical Research Letters*, Vol. 32, L19802

Lipa, B.J., Barrick, D.E., Bourg, J. & Nyden, B.B. (2006). HF radar detection of tsunamis, *J. Oceanography*, Vol. 62, 705-716

Lognonne, P., Garcia, R., Crespon, F., Occipinti, G., Kherani, A. and Artru-Lambin, J. (2006). Seismic waves in the ionosphere. *Europhysics*, Vol.37, No.4, 11-14

Marquart, N. (2007). *Concept study about new ground-based and space-borne HF and microwave systems for tsunami detection.* DLR Microwaves and Radar Institute Project GITEWS Concept Study Report, GITEWS-HF-DLR-001

Najita, K., Weaver, P. & Yuen, P.C. (1974). A tsunami warning system using and ionospheric technique. *Proceedings of the IEEE*, Vol.62, No.5, 563-567

NOAA (2010). http://www.ndbc.noaa.gov/dart.shtml

Occipinti, G., Dorey, P., Bazin, V. & Lognonne, P. (2004). Nostradamus : a new ionospheric seismometer, *Proceedings of the IEEE International Radar Conference*, Toulouse, 2004

Occipinti, G., Lognonne, P., Kherani, E.A. & Hebert, H. (2006). Three-dimensional waveform modelling of ionospheric signature induced by the 2004 Sumatra tsunami. *Geophysical Research Letters*, Vol. 33, L20104

Occhipinti, G., Dorey, P., Farges, T. & Lognonne, P. (2010). Nostradamus: The radar that wanted to be a seismometer. *Geophysical Research Letters*, doi:10.1029/2010GL044009, in press.

Peltier, W.R. & Hines, C.O. (1976). On the possible detection of tsunamis by a monitoring of the ionosphere. *Journal of Geophysical. Research*, Vol. 81, No. 12, 1995-2000

Reddy, N., Aung, T. & Singh, A. (2009). Effect of 2004 'Boxing Day' tsunami on water properties and currents in the Bay of Bengal. *American Journal of Environmental Sciences*, Vol.5, No.3, 247-255

Spitsyn, V.G. & Taraschuk, Y.E. (1994). Filtering in the upper atmosphere of acoustic waves generated by earthquakes. *Geomagnetism and Aeronomy*, Vol.34, No.1, 125-126

Sutcliffe, P. R., & Poole, A.W.V. (1984). Low latitude Pc3 pulsations and associated ionospheric oscillations measured by a digital chirp ionosonde. *Geophysical Research Letterrs*, Vol.11(12), 1172–1175

Troitskaya, Y.I. & Ermakov, S.A. (2006). Manifestations of the Indian Ocean tsunami of 2004 in satellite nadir-viewing radar backscatter variations. *Geophysical Research Letters*, Vol. 33, 2006

Yamashita, T. & Sato, R. (1976). Correlation of tsunami and sub-oceanic Rayleigh wave amplitudes: possibility of the use of the Rayleigh wave in tsunami warming system. Journal of the Physics of the Earth, Vol.24, 397-416

Yeh, H., Liu, P., Briggs, M. and Synolakis, C. (1994). Propagation and amplification of tsunamis at coastal boundaries. *Nature*, Vol.372, 353-355